PCCP

ROYAL SOCIETY OF CHEMISTRY

PAPER

View Article Online
View Journal

Cite this: DOI: 10.1039/d5cp01408e

Harnessing electrochemical CO_2 reduction and assisted water electrolysis *via* constrained thermodynamic modeling†

Jinuk Choi, ‡[a] Hyojung Lim, ‡[a] Subramani Surendran, [a] Seonghyeon Park,[a] Junho Shim,[a] Gyoung Hwa Jeong[ab] and Uk Sim *[abc]

Electrochemical CO_2 reduction reaction (CO_2RR) and assisted water electrolysis (AWE) using organic compounds offer promising pathways for sustainable energy conversion. However, the thermodynamic feasibility and efficiency of these processes are strongly influenced by CO_2 phase transitions (both gaseous and aqueous) and operating conditions, such as temperature and pH. This study systematically examines the thermodynamic behavior of CO_2RR and AWE by calculating Gibbs free energy (ΔG), enthalpy (ΔH), and theoretical potentials (E_{TN} and E_{RE}) over a broad temperature range (0–1000 °C) and varying pH conditions. Pourbaix diagrams for key CO_2-derived products, including CO, hydrocarbons, organic acids, and alcohols, are constructed to assess their stability across different electrochemical environments. The analysis reveals that in aqueous-phase CO_2 systems, equilibrium potentials shift due to the effects of CO_2 speciation. In alkaline conditions, dissolved CO_2 undergoes sequential conversion into HCO_3^- and CO_3^{2-}, resulting in increased overpotentials in CO_2RR. Conversely, gaseous CO_2 maintains a stable equilibrium potential, mitigating pH-induced fluctuations that could hinder reaction selectivity and efficiency. In AWE, the phase transition during reaction conditions lowers oxidation potentials, resulting in enhanced energy efficiency. The calculated V_{TN} and V_{RE} values demonstrate that organic oxidation reactions in AWE require substantially lower energy inputs than conventional oxygen evolution reactions, providing a thermodynamic advantage for energy-efficient hydrogen production. This study establishes a comprehensive thermodynamic framework for CO_2 electrochemical conversion, integrating Pourbaix diagrams and temperature-dependent electrochemical modeling to optimize reaction conditions and energy efficiency. These insights contribute to the rational design of electrocatalytic systems and the development of scalable CO_2 conversion technologies for industrial applications.

Received 14th April 2025,
Accepted 6th June 2025

DOI: 10.1039/d5cp01408e

rsc.li/pccp

Introduction

The transition toward sustainable energy systems has become a critical challenge, driven by the urgent need to mitigate greenhouse gas emissions and establish carbon-neutral production pathways. Among various approaches, electrochemical CO_2 conversion has gained significant attention due to its ability to integrate renewable energy sources and enable decentralized chemical synthesis of value-added carbon-based products.[1] However, despite its potential, electrochemical CO_2 reduction reaction (CO_2RR) and assisted water electrolysis (AWE) still face significant energy efficiency and selectivity challenges.[2,3]

Electrochemical CO_2RR enables transformation of CO_2 into fuels and valuable chemicals, such as carbon monoxide (CO), hydrocarbons, organic acids, and alcohols.[4,5] However, its practical implementation remains hindered by high energy requirements, slow reaction kinetics, and issues with product selectivity. The efficiency and selectivity of CO_2RR are strongly influenced by key thermodynamic factors, including CO_2 phase transitions (gaseous *vs.* aqueous), temperature variations, and the composition of the electrolyte.[6–8] While previous studies have explored CO_2RR under different electrolyte conditions, the systematic thermodynamic impact of CO_2 phase transitions and temperature changes has not been thoroughly analyzed.

AWE has been investigated as an alternative to the conventional oxygen evolution reaction (OER) to enhance the overall energy efficiency of the water electrolysis systems.[9,10] In AWE,

[a] *Hydrogen Energy Technology Laboratory, Korea Institute of Energy Technology (KENTECH), 58330 Naju, Republic of Korea. E-mail: usim@kentech.ac.kr*
[b] *Research Institute, NEEL Sciences, INC, Naju, Republic of Korea*
[c] *College of Chemistry and Chemical Engineering, Henan Key Laboratory of Function-Oriented Porous Materials, Luoyang Normal University, Luoyang 471934, China*

† Electronic supplementary information (ESI) available. See DOI: https://doi.org/10.1039/d5cp01408e

‡ These authors contributed equally to this work.

organic oxidation reactions replace OER, reducing the overall voltage requirement for hydrogen production. The feasibility of AWE depends on the oxidation potential of organic compounds, which varies with pH and temperature. While CO_2RR and AWE are fundamentally distinct processes, they share common thermodynamic principles that allow a systematic comparison within the same framework.

A critical challenge in energy conversion research, including CO_2RR, is shifting beyond conventional Faradaic efficiency (FE) assessments to incorporate voltage efficiency (VE) and overall energy efficiency (EE).[11,12] While FE has traditionally been used to evaluate CO_2RR performance, EE provides a more comprehensive metric by considering the actual electrical energy input relative to the theoretical minimum energy required. However, one significant gap in current research is the inconsistent application of theoretical potential calculations, leading to inaccurate energy efficiency estimates. Moreover, conventional Pourbaix diagrams and theoretical potential calculations are typically constructed under standard conditions (25 °C).[13,14] This method fails to accurately represent the practical operating conditions in experimental and industrial scenarios, where electrochemical systems typically operate at elevated temperatures. Since reaction enthalpy (ΔH) and Gibbs free energy (ΔG) vary with temperature, ignoring temperature dependence can lead to misinterpretations of energy efficiency values, further complicating the optimization of CO_2 conversion technologies.

This study extends thermodynamic Pourbaix diagram analysis to address these gaps by incorporating temperature-dependent electrochemical modeling (25–100 °C) for key organic compounds, including hydrocarbons, alcohols, and organic acids. Additionally, theoretical potentials (E_{TN} and E_{RE}) for CO_2RR and AWE are systematically calculated over a broad temperature range (0–1000 °C). This enables a quantitative evaluation of how the CO_2 phase and operating conditions impact electrochemical performance. By providing a rigorous thermodynamic framework, this study quantifies the impact of CO_2 phase transitions on reaction thermodynamics, evaluates temperature-dependent shifts in equilibrium potentials across CO_2RR and AWE, and establishes a systematic approach for optimizing reaction conditions in practical electrochemical systems. Ultimately, this research contributes to the development of more efficient and selective electrochemical CO_2 conversion technologies by refining thermodynamic analyses, optimizing reaction conditions, and advancing practical energy efficiency strategies for sustainable energy production.

Results and discussion

Thermodynamic modelling

Thermodynamic modeling and Pourbaix diagram calculations were performed using the FactSage software package. The FactPS database was employed to determine the theoretical potential of various electrochemical reactions and to assess the formation of potential byproducts associated with electrochemical energy conversion in aqueous environments (Table S1, ESI†). This study focused on energy conversion reactions occurring in aqueous conditions, particularly CO_2RR and assisted water electrolysis using organic compounds. Pourbaix diagrams were generated over a temperature range from 25 °C (room temperature) to 100 °C (the boiling point of H_2O at 1 atm) to analyze the thermodynamic feasibility of these processes under different operational conditions. To improve the clarity of the Pourbaix diagrams, inevitable byproducts with limited relevance or stability under the investigated conditions were excluded from the calculations.

Calculation formulas

Electrochemical reactions involving charge transfer between reactants are crucial in energy conversion applications. The feasibility of these reactions is governed by thermodynamic parameters such as ΔG, ΔH, and theoretical equilibrium voltage. This study establishes a thermodynamic framework to evaluate the feasibility of CO_2RR and AWE using organic compounds under varying temperatures and pH conditions. A comprehensive understanding of these thermodynamic constraints is essential for optimizing electrochemical CO_2 utilization in practical applications. A general electrochemical reaction involving multiple reactants and products is expressed as:

$$\alpha A + \beta B \rightarrow \gamma C + \delta D \quad (1)$$

The thermodynamic feasibility of a reaction is determined by its Gibbs free energy change ($\Delta_r G^\circ$), calculated using the Gibbs free energy of formation ($\Delta_f G^\circ$) of reactants and products under standard conditions. The equation is given by:

$$\Delta_r G^\circ = \gamma \Delta_f G^\circ_C + \delta \Delta_f G^\circ_D - \alpha \Delta_f G^\circ_A - \beta \Delta_f G^\circ_B \quad (2)$$

If $\Delta_r G^\circ$ is negative, the reaction is thermodynamically favorable and can proceed spontaneously. The maximum electrical work extractable from the reaction is given by:

$$\Delta_r G^\circ = -nFE^\circ \quad (3)$$

where n is the number of electrons transferred, E° is the equilibrium potential, which is also called electromotive force (emf), and F is the Faraday constant (96 485 C mol^{-1}).

Both ΔH and ΔG are temperature-dependent. Kirchhoff's law describes the temperature dependence of reaction enthalpy, and its equation is expressed as:[15]

$$\Delta_r H^\circ(T_2) = \Delta_r H^\circ(T_1) + \int_{T_1}^{T_2} \Delta_r C_p^\circ \mathrm{d}T \quad (4)$$

If the heat capacity change ($\Delta_r C_p^\circ$) is assumed to be constant, this simplifies to:

$$\Delta_r H^\circ(T_2) = \Delta_r H^\circ(T_1) + \Delta_r C_p^\circ (T_2 - T_1) \quad (5)$$

Similarly, the Gibbs free energy at any temperature can be determined using:

$$\Delta_r G^\circ(T) = \Delta_r H^\circ(T) - T\Delta_r S^\circ \quad (6)$$

where $\Delta_r S^\circ$ is the standard entropy change of the reaction.

For CO_2RR, the phase of CO_2 (gas and aqueous) significantly affects reaction feasibility due to pH-dependent speciation. In aqueous systems, CO_2 undergoes equilibrium with bicarbonate (HCO_3^-) and carbonate (CO_3^{2-}), altering the effective reduction potential. The acid–base equilibrium is given by:

$$K_a = \frac{[HCO_3^-][H^+]}{CO_2} = e^{-\Delta G^\circ/RT} \quad (7)$$

$$pK_a = -\log_{10}(K_a) = \frac{\Delta G^\circ}{2.303RT} \quad (8)$$

where R is the universal gas constant, and T is the temperature in Kelvin. This equilibrium shift is fundamental in aqueous CO_2RR, where higher pH values promote bicarbonate formation, increasing the reduction overpotential. In contrast, gaseous CO_2 does not undergo phase-dependent changes, maintaining a stable equilibrium potential across pH. For AWE, aqueous CO_2 systems can benefit from this pH-dependent shift in oxidation potential. As the oxidation potential decreases under alkaline conditions, AWE can proceed with lower energy input, making it more favorable than traditional water splitting.

The van't Hoff equation describes how equilibrium constants (K) shift with temperature, particularly relevant for reactions involving solubility equilibria, which is given by:[15]

$$\frac{d\ln K}{dT} = \frac{\Delta_r H^\circ}{RT^2} \quad (9)$$

where K is the equilibrium constant and $\Delta_r H^\circ$ is the reaction enthalpy change. For endothermic reactions ($\Delta H^\circ > 0$), the equilibrium shifts toward the products at higher temperatures, while for exothermic reactions ($\Delta H^\circ < 0$), the equilibrium shifts toward the reactants. This directly impacts CO_2RR and AWE, influencing the feasibility of reactions at elevated temperatures.

The thermodynamic reversible voltage (E_{RE}) defines the minimum potential required for an electrochemical reaction and is calculated as:

$$E_{RE} = -\frac{\Delta G^\circ}{nF} \quad (10)$$

The ΔG change at 25 °C for water electrolysis is 237.1 kJ mol^{-1}, yielding E_{RE} = 1.23 V.

The thermoneutral voltage (E_{TN}) accounts for total enthalpy change (ΔH°), including both electrical and thermal energy:

$$E_{TN} = -\frac{\Delta H^\circ}{nF} \quad (11)$$

For water electrolysis, ΔH° = 286.0 kJ mol^{-1}, resulting in E_{TN} = 1.48 V. In practical applications, the actual operating voltage lies between E_{RE} (1.23 V) and E_{TN} (1.48 V), influenced by kinetic overpotentials and system inefficiencies.

To determine the feasibility of the reaction under non-standard conditions, the Nernst equation is applied:

$$E = E^\circ - \frac{RT}{nF}\ln Q \quad (12)$$

where Q is the reaction quotient, representing the ratio of reactant and product activities. At elevated temperatures, the $-RT/nF \times \ln Q$ term becomes more significant, impacting equilibrium potential and selectivity.

This section presents the fundamental thermodynamic equations for evaluating electrochemical CO_2 conversion and AWE under varying temperature and pH conditions. A comprehensive thermodynamic framework is developed by integrating Gibbs free energy, enthalpy, equilibrium potential, and reaction equilibria. These calculations form the foundation for the Pourbaix diagrams and theoretical potential analyses in the subsequent sections of this study.

CO_2 reduction reactions to CO and hydrocarbons

The electrochemical CO_2RR presents a promising pathway for converting CO_2 into valuable organic compounds under sustainable conditions.[16–19] The efficiency and selectivity of CO_2RR are highly dependent on thermodynamic feasibility, electrolyte composition, CO_2 phase (gaseous and aqueous), and operating temperature. To comprehensively assess these factors, this study constructs Pourbaix diagrams. It calculates thermodynamic voltages (E_{TN} and E_{RE}) for various CO_2-derived products, including CO, hydrocarbons (CH_4, C_2H_4, C_2H_6), organic acids (formic acid and acetic acid), and alcohols (CH_3OH, CH_3CH_2OH, and $C_2H_6O_2$).

The feasibility of CO_2RR is fundamentally dictated by the standard reduction potentials of key electrochemical half-reactions, which determine the minimum voltage required for CO_2 conversion. A critical distinction arises between gaseous and aqueous CO_2 reduction systems due to their differing equilibrium behaviors. In gaseous-phase CO_2 systems, the standard reduction potentials remain independent of pH, as CO_2 does not undergo phase transformation in solution. Conversely, in aqueous-phase systems, CO_2 speciation shifts dynamically with pH, resulting in changes in equilibrium potential that impact reaction efficiency.

Under standard conditions, the reduction of gaseous CO_2 proceeds through multiple proton–electron transfer steps, resulting in the formation of CO, CH_4, C_2H_4, and C_2H_6. The equilibrium potentials for these reactions remain independent of pH, as CO_2 in the gas phase does not undergo speciation. The corresponding half-reactions at standard conditions (25 °C, 1 atm) are expressed as follows:[20]

$$CO_2(g) + 2H^+(aq) + 2e^- \rightleftharpoons CO(g) + H_2O(l), \quad E^\circ = -0.104\ \text{V } \textit{vs.}\ \text{SHE} \quad (13)$$

$$CO_2(g) + 8H^+(aq) + 8e^- \rightleftharpoons CH_4(g) + 2H_2O(l), \quad E^\circ = 0.169\ \text{V } \textit{vs.}\ \text{SHE} \quad (14)$$

$$2CO_2(g) + 12H^+(aq) + 12e^- \rightleftharpoons C_2H_4(g) + 4H_2O(l), \quad E^\circ = 0.079\ \text{V } \textit{vs.}\ \text{SHE} \quad (15)$$

$$2CO_2(g) + 14H^+(aq) + 14e^- \rightleftharpoons C_2H_6(g) + 4H_2O(l), \quad E^\circ = 0.143\ \text{V } \textit{vs.}\ \text{SHE} \quad (16)$$

These reactions illustrate that the electrochemical reduction of gaseous CO_2 requires an external potential input to drive

product formation under standard conditions. The overall energy demand is dictated by the number of protons and electrons involved, with methane production requiring the highest charge transfer. As shown in Fig. S1 (ESI†), the stability of equilibrium potentials across varying pH levels makes gaseous CO_2 advantageous for maintaining consistent reaction selectivity. However, these theoretical potentials should be applied exclusively to gas-phase reactions, as aqueous systems require consideration of CO_2 phase transitions and related speciation effects.

In aqueous-phase systems, CO_2 undergoes pH-dependent speciation, leading to the formation of HCO_3^- and CO_3^{2-}, which significantly impact the thermodynamics of the reduction reaction. The half-reactions for aqueous-phase CO_2 reduction under standard conditions are as follows:

$$CO_2(aq) + 2H^+(aq) + 2e^- \rightleftharpoons CO(aq) + H_2O(l), \quad E^\circ = -0.150\ \text{V } \textit{vs.}\ \text{SHE} \tag{17}$$

$$CO_2(aq) + 8H^+(aq) + 8e^- \rightleftharpoons CH_4(aq) + 2H_2O(l), \quad E^\circ = -0.159\ \text{V } \textit{vs.}\ \text{SHE} \tag{18}$$

$$2CO_2(aq) + 12H^+(aq) + 12e^- \rightleftharpoons C_2H_4(aq) + 4H_2O(l), \quad E^\circ = 0.083\ \text{V } \textit{vs.}\ \text{SHE} \tag{19}$$

$$2CO_2(aq) + 14H^+(aq) + 14e^- \rightleftharpoons C_2H_6(aq) + 4H_2O(l), \quad E^\circ = 0.144\ \text{V } \textit{vs.}\ \text{SHE} \tag{20}$$

Fig. 1 presents Pourbaix diagrams of CO and hydrocarbons (CH_4, C_2H_4, and C_2H_6) across various temperatures (25–100 °C), providing insights into the pH-dependent stability of CO_2 reduction products in aqueous conditions and the electrochemical potential required for selective hydrocarbon formation. The equilibrium potential for CO_2 reduction in aqueous systems is strongly influenced by pH, particularly under alkaline conditions, where CO_2 undergoes speciation into HCO_3^- and CO_3^{2-}. This phase-dependent shift increases the required overpotential for CO_2RR, making reduction reactions less favorable in basic environments.

In contrast, gaseous CO_2 maintains stable equilibrium potentials across different pH values, as it does not undergo speciation changes (Fig. S1, ESI†). This stability enhances reaction selectivity and minimizes pH-induced fluctuations that could hinder efficiency. To account for these phase differences, Pourbaix diagrams were constructed for both gas-phase and aqueous-phase CO_2 systems. The graphs illustrate key phase boundaries, showing that the pK_a values for CO_2(aq) to HCO_3^- are 6.381, 6.288, and 6.205, while those for HCO_3^- to CO_3^{2-} are 10.329, 10.194, and 10.243 at 25 °C, 50 °C, and 100 °C, respectively. These values indicate a strong pH

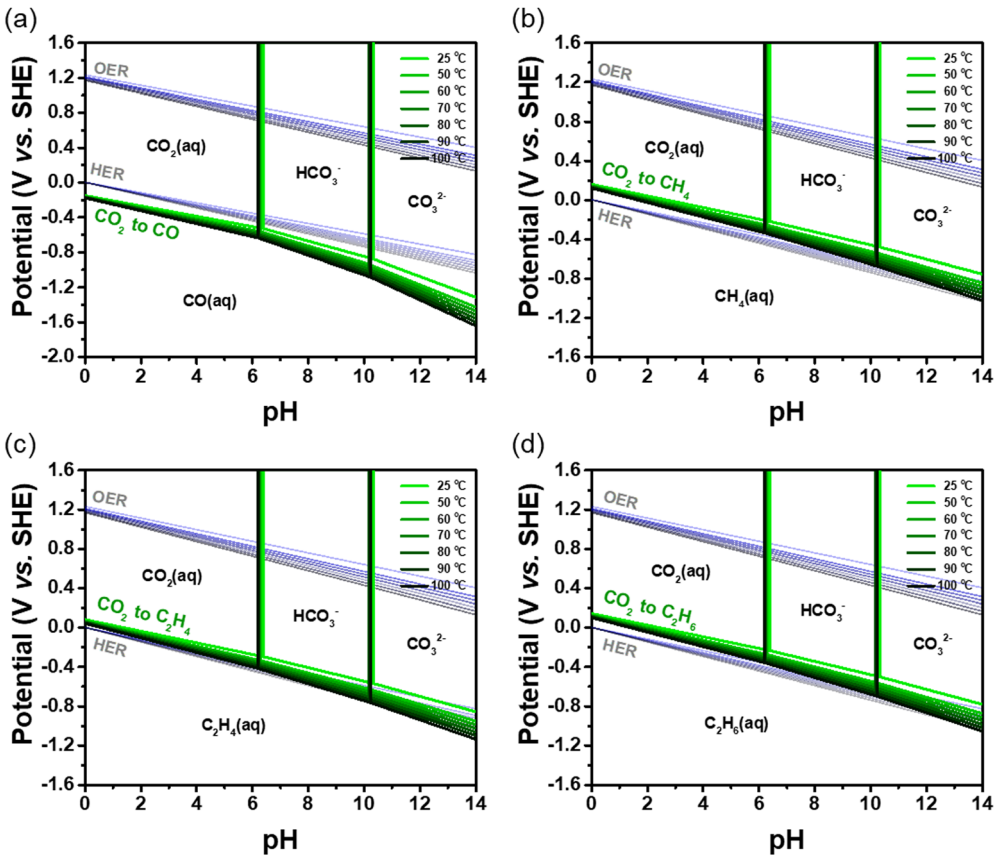

Fig. 1 Pourbaix diagrams of hydrocarbons including (a) CO, (b) CH_4, (c) C_2H_4, and (d) C_2H_6 using CO_2(aq) as a function of temperature from 25 to 100 °C.

dependency in aqueous systems, resulting in significant shifts in equilibrium potential with increasing pH.

A comparison of gaseous and aqueous CO_2 reduction underscores the importance of selecting optimal phase and electrolyte conditions to maximize conversion efficiency. While gaseous CO_2 enables stable equilibrium potentials, aqueous-phase CO_2 introduces pH-dependent shifts that influence reduction and oxidation pathways, affecting reaction efficiency and selectivity. The reduction potentials for CO_2-to-CO conversion are −0.150 V and −1.312 V *vs.* SHE at pH 0 and pH 14, respectively, at 25 °C (Fig. 1(a)). As temperature increases to 100 °C, these potentials decrease further to −0.176 V and −1.640 V *vs.* SHE at pH 0 and pH 14, respectively. For CO_2-to-CH_4 reduction, the equilibrium potentials are 0.159 V at pH 0 and −0.753 V at pH 14 at 25 °C (Fig. 1(b)). These values decrease to 0.122 V and −1.021 V *vs.* SHE at 100 °C. Similarly, for CO_2-to-C_2H_4 reduction, the equilibrium potentials at 25 °C are 0.083 V at pH 0 and −0.857 V at pH 14 (Fig. 1(c)), shifting further down to 0.044 V and −1.135 V at 100 °C. Lastly, for CO_2-to-C_2H_6 reduction, the equilibrium potentials are 0.144 V at pH 0 and −0.780 V at pH 14 at 25 °C (Fig. 1(d)). These values decrease to 0.103 V and −1.056 V at 100 °C. The trends of the CO_2-to-CO, CH_4, C_2H_4, and C_2H_6 reactions indicate that under aqueous conditions, the theoretical reduction potentials become more hostile as pH increases after CO_2 transitions to the HCO_3^- and CO_3^{2-} phases, leading to higher overpotentials for CO_2RR in neutral and alkaline environments. This increased overpotential negatively impacts the efficiency of CO_2 reduction, making CO_2RR less favorable under basic conditions.

Fig. 2 compares the potential gap ($E_{CO_2RR} - E_{HER}$) between aqueous CO_2RR and hydrogen evolution reaction (HER) across various pH and temperature conditions. The results highlight that while it thermodynamically hinders CO_2-to-CO conversion under all conditions, CO_2-to-CH_4, –C_2H_4, and –C_2H_6 exhibit potential windows where HER competition is minimized, suggesting an optimal pH range for selective hydrocarbon formation. The CO_2-to-CO reaction is unable to avoid HER competition at any pH or temperature (Fig. 2(a)). The potential gaps between CO_2-to-CO and HER are −0.150 V and −0.484 V, respectively, at pH 0 and pH 14, at 25 °C. As the temperature increases to 100 °C, these potential gaps further decrease to −0.176 V and −0.604 V at pH 0 and pH 14, respectively.

In contrast, the CO_2-to-CH_4 reaction exhibits a CO_2RR-dominant region across all pH levels within the 25–100 °C temperature range (Fig. 2(b)). The potential gaps between CO_2-to-CH_4 and HER are 0.159 V and 0.076 V, respectively, at pH 0

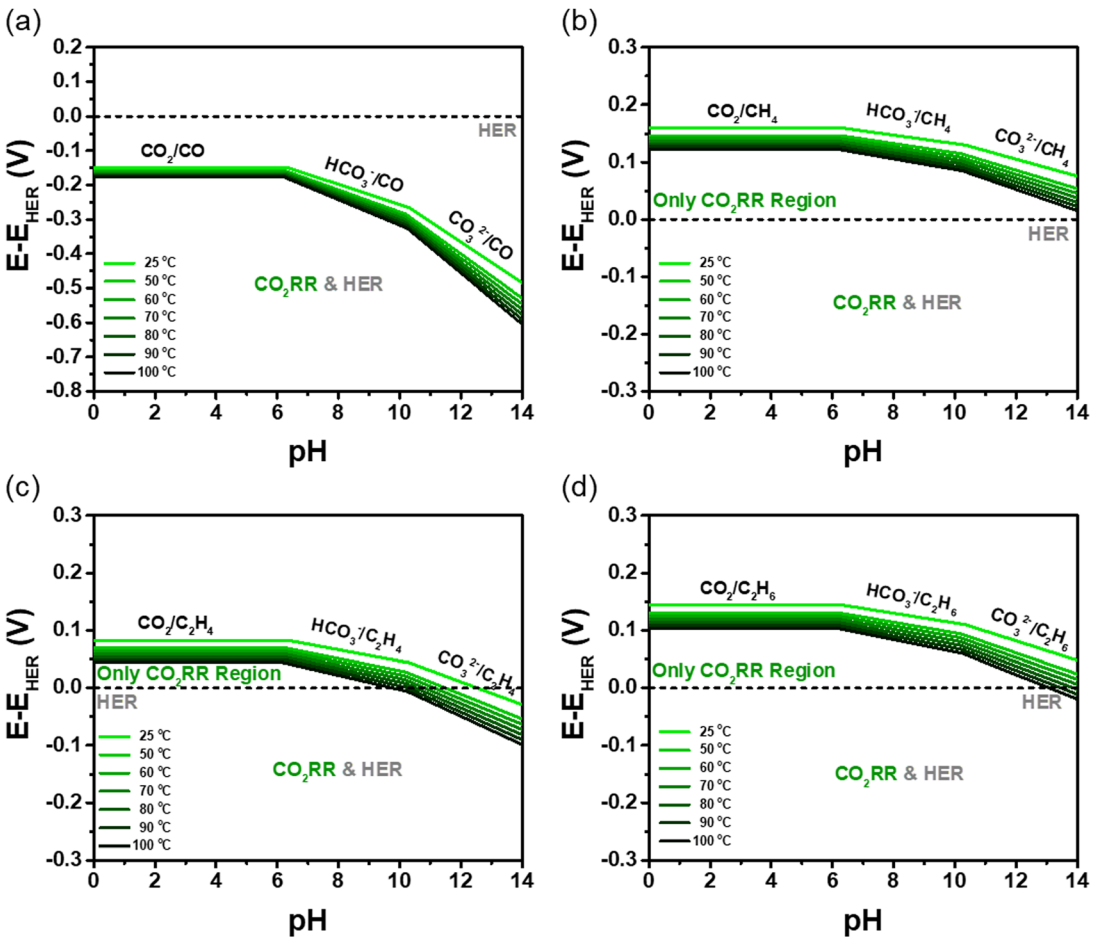

Fig. 2 Potential gap between CO_2RR and HER for the formation of (a) CO, (b) CH_4, (c) C_2H_4, and (d) C_2H_6 as a function of temperature (25–100 °C).

and pH 14, at 25 °C. As the temperature increases to 100 °C, these potential gaps further decrease to 0.122 V and 0.016 V at pH 0 and pH 14, respectively. In contrast, the CO_2-to-CH_4 reaction exhibits a CO_2RR-dominant region across all pH levels within the 25–100 °C temperature range (Fig. 2(b)). The potential gaps between CO_2-to-CH_4 and HER are 0.159 V and 0.076 V, respectively, at pH 0 and pH 14, at 25 °C. As the temperature increases to 100 °C, these potential gaps further decrease to 0.122 V and 0.016 V at pH 0 and pH 14, respectively. Notably, within the pH range of 0 to 6.381 at 25 °C, the largest potential gap (0.159 V) between CO_2RR and HER is observed. These conditions provide a wide operating window where HER can be suppressed, thereby improving the selectivity and efficiency of CO_2RR.

Similarly, the CO_2-to-C_2H_4 reaction predominantly occurs within the CO_2RR region, except under strongly basic conditions (Fig. 2(c)). As the temperature increases, the exclusive CO_2RR region gradually diminishes. The potential gaps between CO_2-to-C_2H_4 and HER are 0.083 V and −0.028 V, respectively, at pH 0 and pH 14, at 25 °C. At 100 °C, these potential gaps decrease to 0.044 V and −0.099 V at pH 0 and 14, respectively. The CO_2-to-C_2H_6 reaction follows a trend similar to that of CO_2-to-CH_4, maintaining a large CO_2RR-dominant region (Fig. 2(d)). However, at temperatures exceeding 80 °C, HER becomes unavoidable under strongly basic conditions. The potential gaps between CO_2-to-C_2H_6 and HER are 0.144 V and 0.048 V, respectively, at pH 0 and pH 14, at 25 °C. As the temperature increases to 100 °C, these potential gaps further decrease to 0.103 V and −0.019 V at pH 0 and pH 14, respectively. These thermodynamic analyses provide deeper insights into reaction mechanisms, enabling improved efficiency and guiding the selection of optimal operating temperatures and pH conditions for practical applications.

Fig. 3 presents the theoretical potential trends for CO_2 reduction to CO and hydrocarbons over a temperature range of 0–1000 °C. The V_{RE} and V_{TN} define the minimum and total energy requirements, respectively, under ideal conditions. For CO_2-to-CO conversion, below 100 °C, both V_{TN} and V_{RE} decrease as temperature increases (Fig. 3(a)). The calculated V_{RE} for CO_2-to-CO remains higher than that of HER/OER. At the same time, V_{TN} is comparable to HER/OER, indicating unavoidable HER competition during CO_2RR for CO formation. However, beyond 100 °C, V_{RE} for CO_2-to-CO begins to decrease, eventually crossing below the V_{RE} of HER/OER at approximately 800 °C, suggesting a shift in thermodynamic favorability. Additionally, the Fischer–Tropsch process, which involves the conversion of CO to hydrocarbons, was analyzed over a temperature range of 0–1000 °C (Fig. S2, ESI†). This process is highly temperature-dependent, with temperature control critical in product distribution and reaction efficiency. Fig. 3(b) compares the V_{TN} and V_{RE} values for CO_2-to-hydrocarbon conversion, including CH_4, C_2H_4, and C_2H_6, with those of HER/OER over a broad temperature range (0–1000 °C). At 25 °C, the V_{TN} values for CH_4/OER (1.153 V), C_2H_4/OER (1.219 V), and C_2H_6/OER (1.155 V) are significantly lower than that of HER/OER (1.481 V). Similarly, the V_{RE} values at 25 °C for CH_4/OER (1.060 V), C_2H_4/OER (1.150 V), and C_2H_6/OER (1.086 V) are also considerably lower than that of HER/OER (1.229 V). These lower theoretical potentials for CO_2-to-hydrocarbon conversion indicate a competitive advantage over hydrogen evolution, as the reduction of CO_2 to hydrocarbons occurs at a lower potential than HER/OER. This suggests that hydrocarbon formation at 25 °C could be selectively favored over hydrogen production, depending on the applied electrochemical conditions.

As the temperature increases to 100 °C, the theoretical potentials for all reactions decrease. However, beyond 100 °C, the theoretical potentials gradually increase with temperature, except for V_{RE} of C_2H_4/OER and HER/OER, which continue to decline. At temperatures above 600 °C, the V_{RE} of CO_2-to-hydrocarbon conversion exceeds that of HER/OER, indicating that hydrogen evolution becomes thermodynamically unavoidable in this temperature range. However, from the perspective of V_{TN}, CO_2-to-hydrocarbon conversion still maintains a lower potential than HER/OER, suggesting that despite the inherent competition with HER at high temperatures, hydrocarbon formation remains thermodynamically viable. These thermodynamic understandings provide a fundamental understanding of the temperature-dependent feasibility of CO_2RR and

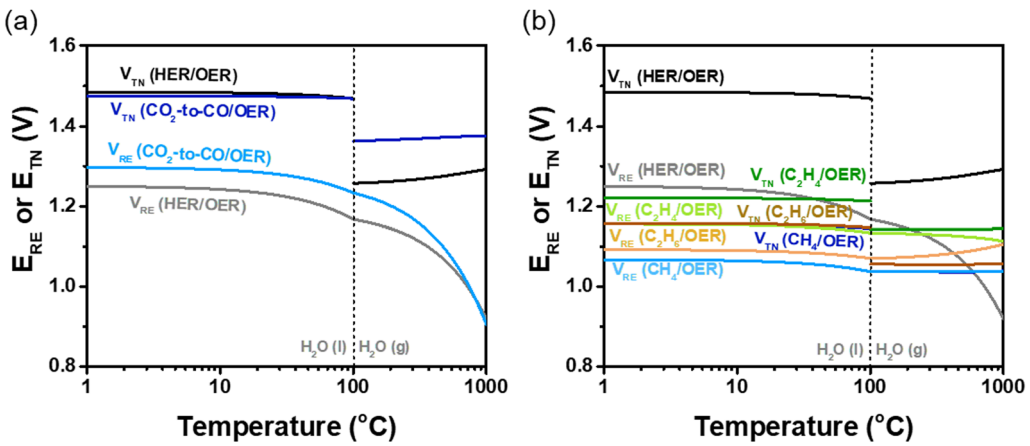

Fig. 3 Theoretical potentials (V_{TN} and V_{RE}) of (a) CO_2RR to CO and (b) hydrocarbons, as a function of temperature from 0 to 1000 °C.

hydrocarbon synthesis, offering guidance for optimizing electrocatalytic CO_2 conversion under practical operating conditions.

CO_2 reduction reactions to organic acids

Electrochemical CO_2 reduction can produce hydrocarbons and organic acids, which are significant in various industrial applications.[21,22] Understanding the thermodynamic feasibility of these reactions is essential for optimizing selectivity and efficiency in CO_2 conversion systems. Fig. 4 presents a thermodynamic analysis of CO_2 reduction to organic acids, specifically formic acid (HCOOH) and acetic acid (CH_3COOH), as a function of pH and temperature. The Pourbaix diagrams illustrate variations in equilibrium potential, while the potential gap analysis highlights the competition between CO_2RR and HER. Given the similar trends observed in CO_2-to-hydrocarbon conversions, except in certain regions due to product phase changes, understanding these thermodynamic constraints is crucial for optimizing CO_2RR selectivity under varying electrochemical conditions. Under standard conditions, the reduction of gaseous CO_2 proceeds *via* multiple proton–electron transfer steps, forming HCOOH and CH_3COOH. Since gaseous CO_2 does not undergo pH-dependent speciation, its equilibrium potential remains stable across all pH conditions, providing a consistent reaction environment. However, in practical electrochemical CO_2RR systems, CO_2 is typically dissolved in aqueous electrolytes, where it undergoes acid–base equilibria, forming HCO_3^- and CO_3^{2-} species. This conversion has a significant impact on electrochemical behavior, altering the equilibrium potential as a function of pH. The half-reactions for organic acid formation from gaseous and aqueous CO_2 are as follows:[23]

$$CO_2(g) + 2H^+(aq) + 2e^- \rightleftharpoons HCOOH(aq), \quad E^\circ = -0.114\ \text{V } \textit{vs.}\ \text{SHE} \tag{21}$$

$$2CO_2(g) + 8H^+(aq) + 8e^- \rightleftharpoons CH_3COOH(aq) + H_2O(l), \quad E^\circ = -0.106\ \text{V } \textit{vs.}\ \text{SHE} \tag{22}$$

$$CO_2(aq) + 2H^+(aq) + 2e^- \rightleftharpoons HCOOH(aq), \quad E^\circ = -0.071\ \text{V } \textit{vs.}\ \text{SHE} \tag{23}$$

$$2CO_2(aq) + 8H^+(aq) + 8e^- \rightleftharpoons CH_3COOH(aq) + H_2O(l), \quad E^\circ = 0.128\ \text{V } \textit{vs.}\ \text{SHE} \tag{24}$$

These results indicate that aqueous-phase CO_2RR exhibits a slight increase in equilibrium potential compared to its gaseous counterpart, potentially lowering the overpotential requirements for organic acid production. However, at higher

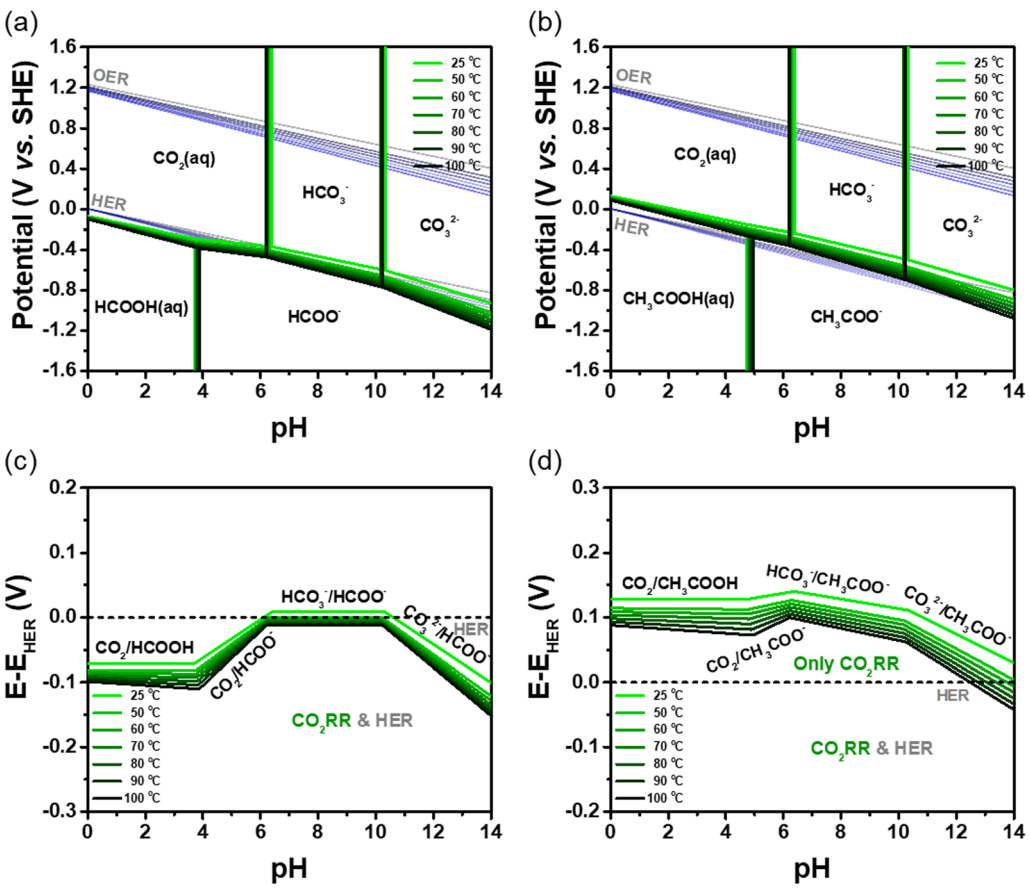

Fig. 4 Pourbaix diagrams of organic acids, including (a) formic acid and (b) acetic acid, using CO_2(aq) as a function of temperature from 25 to 100 °C. Potential gap between CO_2RR and HER for the formation of (c) HCOOH and (d) CH_3COOH as a function of temperature (25–100 °C).

pH levels, the dominance of HCO_3^- and CO_3^{2-} leads to increased overpotential requirements, reducing conversion efficiency.

As shown in Fig. 4(a), the Pourbaix diagram for CO_2-to-HCOOH conversion exhibits temperature dependence and significant variations across intermediate pH values due to CO_2 speciation ($CO_2(aq) \rightleftharpoons HCO_3^- \rightleftharpoons CO_3^{2-}$) and the acid–base equilibrium of HCOOH. The dissociation of HCOOH into formate ($HCOO^-$) follows a pK_a of 3.7153, 3.7357, and 3.8693 at 25, 50, and 100 °C, respectively, introducing a noticeable inflection point in this pH range, which further alters the thermodynamic favorability of HCOOH formation.

A similar trend is observed in Fig. 4(b) for CO_2-to-CH_3COOH conversion, where the equilibrium potential exhibits significant variations at intermediate pH due to CO_2 speciation effects and the acid–base equilibrium of CH_3COOH. The dissociation of CH_3COOH into acetate (CH_3COO^-) follows pK_a values of 4.7347, 4.7655, and 4.944 at 25, 50 °C, and 100 °C, leading to a distinct inflection point within this pH range, influencing the reaction energetics.

Compared to CO_2-to-hydrocarbon conversions, these organic acid formation reactions involve an additional acid–base equilibrium step, resulting in more pronounced variations in equilibrium potential across different pH regions. This increased complexity introduces multiple transition points, making the thermodynamic landscape of CO_2-to-organic acid conversion more complex than that of hydrocarbon formation. Therefore, a more precise thermodynamic analysis is required for accurate predictions.

While the Pourbaix diagrams provide valuable insights into equilibrium, they do not account for HER competition under practical conditions. Fig. 4(c) and (d) compare the potential gaps between CO_2RR and HER, identifying selective reaction regions where CO_2RR is thermodynamically favored. As shown in Fig. 4(c), the equilibrium potential of HER is more favorable than that of CO_2-to-HCOOH, making HER the thermodynamically favored reaction under most conditions. Consequently, HER dominates across a wide pH range, significantly lowering the faradaic efficiency of HCOOH production. However, within a moderate pH range (~6–11) at temperatures below 50 °C, the equilibrium potential for CO_2-to-HCOOH, which is effectively governed by the HCO_3^-/$HCOO^-$ equilibrium, shifts more positive than that of HER, partially suppressing HER and enabling a selective CO_2RR region. As temperature increases, this selective window narrows, reducing the effectiveness of CO_2RR. In contrast, Fig. 4(d) shows that CO_2-to-CH_3COOH conversion occurs predominantly at more positive equilibrium potentials, making it less susceptible to HER competition except under highly basic and high-temperature conditions. Since CH_3COOH formation requires multiple proton–electron transfer steps, it exhibits a larger overpotential window relative to HER, reducing unwanted H_2 evolution. As a result, CH_3COOH production remains selective across a broader pH range. However, at temperatures exceeding 60 °C, a slight downward shift in equilibrium potential occurs under highly basic conditions (pH > 13–14), leading to partial HER overlap. Despite this, CH_3COOH formation remains unaffected mainly by HER, maintaining a high selectivity window for CO_2RR.

These results highlight the substantial influence of pH and temperature on CO_2RR selectivity. The analysis indicates that HCOOH formation is highly susceptible to HER competition due to its equilibrium potential being close to that of HER, significantly reducing its faradaic efficiency. In contrast, CH_3COOH demonstrates a broader CO_2RR-selective window, making it a more viable candidate for practical electrochemical CO_2 conversion applications. Therefore, precise optimization of temperature and pH conditions is essential to enhance CO_2RR selectivity while minimizing HER interference.

The calculated V_{RE} and V_{TN} for CO_2RR to organic acids are compared in Fig. 5, providing insights into the competition between CO_2RR and HER under varying temperature conditions (0–1000 °C). Evaluating the thermodynamic feasibility of CO_2RR in relation to water electrolysis is crucial for optimizing reaction selectivity and energy efficiency in electrochemical CO_2 conversion. At 25 °C, the V_{RE} values for HCOOH/OER (1.410 V) and CH_3COOH/OER (1.132 V) are both lower than that of HER/OER (1.229 V). However, the V_{RE} of HCOOH/OER is higher than that of HER/OER, indicating unavoidable competition with HER during formic acid formation. Conversely, the V_{TN} values at 25 °C for HCOOH/OER (1.329 V) and CH_3COOH/OER (1.133 V) are significantly lower than that of HER/OER (1.481 V). This suggests that CO_2-to-organic acid conversion occurs at a lower thermodynamic threshold than HER/OER, reducing direct competition with HER and improving selectivity under practical electrochemical conditions. The V_{TN} of the CO_2RR for organic acid is lower than the V_{RE} of the reactions, unlike the trends of HER/OER.

As the temperature increases to 100 °C, both V_{RE} and V_{TN} for CO_2-to-organic acid conversion remain lower than those of HER/OER, respectively, indicating a thermodynamically favorable pathway. However, beyond 100 °C, the V_{TN} of HER/OER becomes lower than that of CO_2-to-CHOOH, demonstrating that HER is unavoidable during CO_2RR for CHOOH formation. Additionally, the V_{RE} of CO_2-to-CH_3COOH exceeds that of HER/OER from approximately

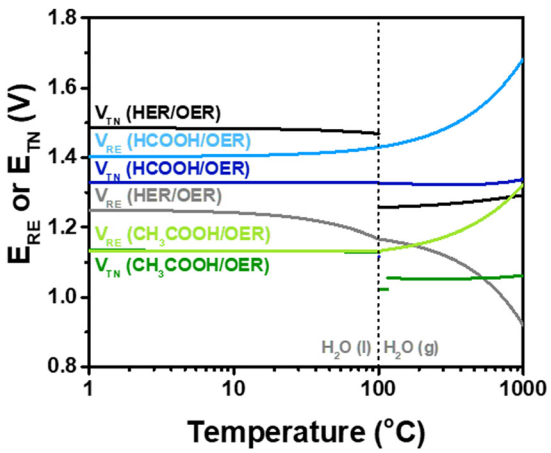

Fig. 5 Theoretical potentials (V_{TN} and V_{RE}) of CO_2RR to organic acids, as a function of temperature from 0 to 1000 °C.

160 °C, further emphasizing the thermodynamic limitations of organic acid formation under high-temperature conditions.

The potential window for CO_2 reduction before HER competition is depicted, revealing that a larger V_{TN} gap between HER/OER and CO_2RR/OER favors CO_2RR in terms of thermodynamic feasibility. These results highlight that HER competition is less dominant in these regions, underscoring the crucial role of enthalpy in governing reaction selectivity. Thus, the thermodynamic analysis of CO_2RR, integrating Pourbaix diagrams and theoretical voltage calculations, provides critical insights into product stability, reaction feasibility, and temperature-dependent behavior. Extending the analysis beyond standard conditions (25 °C), this study establishes a practical framework for designing high-efficiency CO_2 conversion systems, optimizing hydrocarbon and organic acid production under industrially relevant conditions.

CO_2 reduction reactions to alcohols

The electrochemical reduction of CO_2 to alcohols, including methanol (CH_3OH), ethanol (C_2H_5OH), and ethylene glycol ($C_2H_6O_2$), has also been widely studied.[24] These reactions follow a multi-electron, multi-proton transfer pathway, with equilibrium potential shifts primarily governed by pH and temperature. Like hydrocarbon formation, these reactions are influenced by CO_2 speciation ($CO_2(aq) \rightleftharpoons HCO_3^- \rightleftharpoons CO_3^{2-}$), which dictates the thermodynamic feasibility of alcohol production under varying electrochemical conditions. The half-reactions for alcohol formation from gaseous and aqueous CO_2 are as follows:[23,25]

$$CO_2(g) + 6H^+ + 6e^- \rightleftharpoons CH_3OH(aq) + H_2O(l), \quad E^\circ = 0.032\ \text{V } \textit{vs.}\ \text{SHE} \tag{25}$$

$$2CO_2(g) + 2H^+ + 12e^- \rightleftharpoons CH_3CH_2OH(aq) + 3H_2O(l), \quad E^\circ = 0.0902\ \text{V } \textit{vs.}\ \text{SHE} \tag{26}$$

$$2CO_2(g) + 10H^+ + 10e^- \rightleftharpoons C_2H_6O_2(l) + H_2O(l), \quad E^\circ = 0.009\ \text{V } \textit{vs.}\ \text{SHE} \tag{27}$$

$$CO_2(aq) + 6H^+ + 6e^- \rightleftharpoons CH_3OH(aq) + H_2O(l), \quad E^\circ = 0.046\ \text{V } \textit{vs.}\ \text{SHE} \tag{28}$$

$$2CO_2(aq) + 2H^+ + 12e^- \rightleftharpoons CH_3CH_2OH(aq) + 3H_2O(l), \quad E^\circ = 0.105\ \text{V } \textit{vs.}\ \text{SHE} \tag{29}$$

$$2CO_2(aq) + 10H^+ + 10e^- \rightleftharpoons C_2H_6O_2(l) + H_2O(l), \quad E^\circ = 0.030\ \text{V } \textit{vs.}\ \text{SHE} \tag{30}$$

As shown in Fig. 6(a)–(c), the Pourbaix diagrams illustrate the variations in equilibrium potential for the formation of methanol, ethanol, and ethylene glycol as a function of pH and temperature. The formation of alcohols requires the stepwise addition of protons and electrons to CO_2-derived intermediates, with equilibrium potentials strongly influenced by electrolyte pH. As pH increases, CO_2 undergoes a phase transition to HCO_3^- and CO_3^{2-}, shifting the equilibrium potential more negative and increasing the overpotential required for alcohol production.

The equilibrium potentials for CO_2-to-CH_3OH conversion are 0.046 V and −0.894 V *vs.* SHE at pH 0 and pH 14, respectively, at 25 °C (Fig. 6(a)). As temperature increases to 100 °C, these potentials decrease further to 0.007 V and −1.172 V *vs.* SHE at pH 0 and pH 14, respectively. For the reduction of CO_2 to CH_3CH_2OH, the equilibrium potentials at

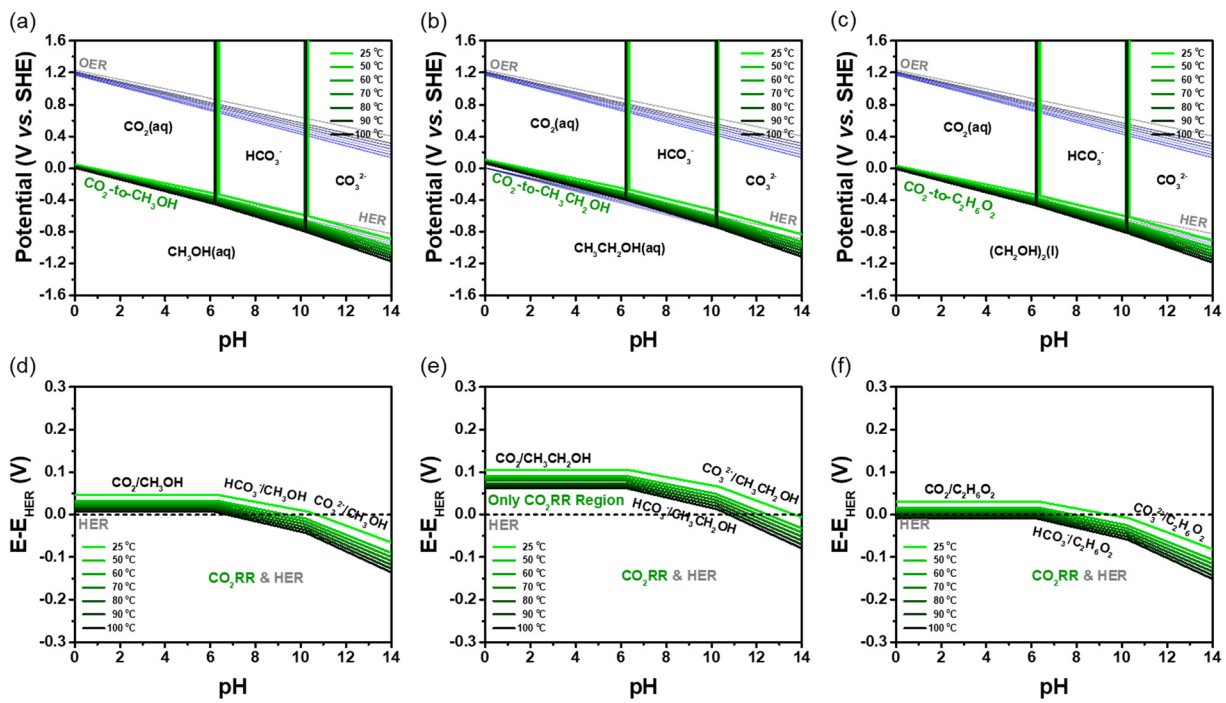

Fig. 6 Pourbaix diagrams of (a) methanol, (b) ethanol, and (c) ethylene glycol as a function of temperature from 25 to 100 °C. The potential gap between CO_2RR and HER for the formation of (d) CH_3OH, (e) CH_3CH_2OH, and (f) $C_2H_6O_2$ as a function of temperature (25–100 °C).

25 °C are 0.105 V at pH 0 and −0.835 V *vs.* SHE at pH 14 (Fig. 6(b)). These values further decrease to 0.063 V and −1.116 V *vs.* SHE at 100 °C. Similarly, for CO_2-to-$C_2H_6O_2$ reduction, the equilibrium potentials at 25 °C are 0.030 V at pH 0 and −0.909 V *vs.* SHE at pH 14 (Fig. 6(c)), shifting further down to −0.009 V and −1.188 V *vs.* SHE at 100 °C. This trend is consistent with CO_2-to-hydrocarbon reduction, where lower pH conditions favor product formation due to CO2 speciation. The stability regions of methanol, ethanol, and ethylene glycol shift toward lower pH values, indicating that their formation is thermodynamically more favorable under acidic conditions. In alkaline environments, the equilibrium potential becomes increasingly negative, making alcohol formation less efficient due to the higher energy input required for reduction.

Fig. 6(d)–(f) compares the potential gaps between CO_2RR for alcohol formation and HER, revealing selective electrochemical windows where alcohol production can be favored over HER. Like hydrocarbons, the formation of alcohol follows a comparable thermodynamic trend, reinforcing the close relationship between CO_2-to-alcohol and CO_2-to-hydrocarbon conversion pathways. Unlike CO_2-to-organic acid conversions, which exhibit distinct transition points due to additional acid–base equilibria of products, alcohol formation is primarily governed by CO_2 speciation and electrolyte pH, resulting in a more continuous thermodynamic shift.

The CO_2-to-CH_3OH reaction avoids HER competition under acidic and neutral conditions, particularly at low temperatures (Fig. 6(d)). The potential gaps ($E_{CO_2RR} - E_{HER}$) between CO_2-to-CH_3OH and HER are 0.046 V and −0.065 V at pH 0 and pH 14, respectively, at 25 °C. As the temperature increases to 100 °C, these potential gaps decrease to 0.007 V and −0.136 V at pH 0 and pH 14, respectively, indicating a reduced thermodynamic driving force for CH_3OH formation at elevated temperatures. The CO_2-to-CH_3CH_2OH reaction exhibits a broader CO_2RR-dominant region than CO_2-to-CH_3OH (Fig. 6(e)). At 25 °C, the potential gaps between CO_2-to-CH_3CH_2OH and HER are 0.105 V at pH 0 and −0.007 V at pH. As the temperature increases to 100 °C, these values decrease to 0.063 V and −0.080 V at pH 0 and pH 14, respectively. These conditions provide a wider operating window, which minimizes HER competition and thereby improves both the selectivity and efficiency of CO_2RR. Among alcohol formation pathways, the CO_2-to-$C_2H_6O_2$ reaction exhibits the narrowest CO_2RR-dominant region (Fig. 6(f)). As temperature and pH increase, this exclusive CO_2RR region gradually diminishes. The potential gaps between CO_2-to-$C_2H_6O_2$ and HER are 0.030 V at pH 0 and −0.081 V at pH 14 at 25 °C, which further decrease to −0.009 V and −0.151 V at 100 °C, respectively. These results highlight the increasing thermodynamic limitations on ethylene glycol formation as temperature and pH rise.

The V_{TN} and V_{RE} for CO_2-to-alcohol conversion were calculated using enthalpy change and Gibbs free energy. Fig. 7 compares the V_{TN} and V_{RE} values for methanol (MeOH), ethanol (EtOH), and ethylene glycol (EgOH) formation with those of HER/OER over a broad temperature range (0–1000 °C). At 25 °C, the V_{RE} values for MeOH/OER (1.213 V), EtOH/OER (1.145 V), and EgOH/OER (1.220 V) are all lower than that of HER/OER (1.229 V). Among them, the V_{RE} of MeOH/OER and EgOH/OER are particularly close to HER/OER, indicating inevitable competition with HER. Conversely, the V_{TN} values at 25 °C for MeOH/OER (1.255 V), EtOH/OER (1.181 V), and EgOH/OER (1.233 V) are significantly lower than that of HER/OER (1.481 V). From the V_{TN} perspective, CO_2-to-alcohol conversion exhibits a lower potential than HER/OER, suggesting that alcohol formation is more thermodynamically favorable than HER at 25 °C, despite the inherent competition with HER. These lower theoretical potentials for CO_2-to-alcohol conversion indicate a competitive advantage over hydrogen evolution, as CO_2 reduction to alcohols occurs at a lower potential than HER/OER. This suggests that alcohol formation at 25 °C could be selectively favored over hydrogen production, depending on the applied electrochemical conditions.

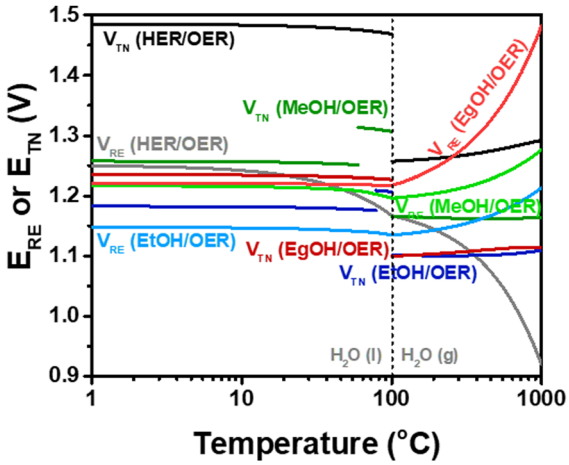

Fig. 7 Theoretical potentials (V_{TN} and V_{RE}) of CO_2-to-alcohol reactions as a function of temperature from 0 to 1000 °C.

As the temperature increases to 100 °C, the theoretical potentials for all reactions decrease. Notably, the V_{RE} of HER/OER decreases rapidly, surpassing the VRE of MeOH/OER and EtOH/OER. Meanwhile, the V_{RE} of EtOH/OER remains consistently lower than that of HER/OER from 0 to 100 °C, suggesting a more favorable electrochemical pathway. Beyond 100 °C, the theoretical potentials gradually increase with temperature, except for V_{RE} of HER/OER, which continues to decline. At temperatures above 350 °C, the V_{RE} of all CO_2-to-alcohol conversions exceeds that of HER/OER, indicating that hydrogen evolution becomes thermodynamically unavoidable in this temperature range. However, from the V_{TN} perspective, CO_2-to-alcohol conversion still maintains a lower potential than HER/OER, except for EgOH/OER, suggesting that despite the inherent competition with HER at high temperatures, alcohol formation remains thermodynamically viable. The findings elucidate the temperature-dependent viability of CO_2RR and alcohol synthesis, providing valuable guidelines for tailoring reaction conditions and enhancing the efficiency of electrocatalytic CO_2 conversion in practical applications.

Assisted water electrolysis using organic compounds

Water electrolysis is a promising method for hydrogen production; however, its widespread application is constrained by the high energy demand of the OER, which is the kinetically sluggish half-reaction. AWE has been explored as an alternative approach to address this challenge, wherein organic oxidation reactions replace OER, thereby reducing the overall cell voltage.[26] The oxidation of organic molecules, such as methanol (MOR), ethanol (EOR), and ethylene glycol (EGOR), has been demonstrated as a more energy-efficient alternative to conventional water splitting.[27–29] Fig. 6(a)–(c) presents the Pourbaix diagrams of methanol, ethanol, and ethylene glycol, depicting the equilibrium potentials for both CO_2-to-alcohol formation and oxidation pathways. Since reduction and oxidation reactions share the same equilibrium potentials, these diagrams provide insights into the feasibility of both processes under various electrochemical conditions.

The feasibility of AWE depends on the electrochemical stability and oxidation potential of organic compounds, both of which vary with pH and temperature. To further analyze the oxidation behavior, Fig. 8 illustrates the calculated oxidation potentials of methanol, ethanol, and ethylene glycol, comparing them with those of conventional water electrolysis. The potential gap between conventional water electrolysis and AWE highlights the energy advantage of organic oxidation. Additionally, the inflection points at pH 6.38 and pH 10.33 correspond to phase transitions of CO_2 species, indicating changes in oxidation behavior as a function of pH. Depending on the applied potential and pH, methanol undergoes electrochemical oxidation to CO_2, HCO_3^-, or CO_3^{2-} (Fig. 8(a)). The data indicate that methanol remains stable under acidic conditions. However, it becomes increasingly susceptible to oxidation at lower potentials in neutral pH environments. At 25 °C, the required potentials for HER/MOR are 0.046 V at pH 0 and −0.065 V at pH 14. As the temperature increases to 100 °C, these values decrease to 0.007 V at pH 0 and −0.136 V at pH 14. In strongly alkaline conditions, the potential gap between water electrolysis and methanol oxidation widens, enabling more efficient oxidation. Notably, methanol oxidation to CO_3^{2-} becomes more favorable in alkaline environments.

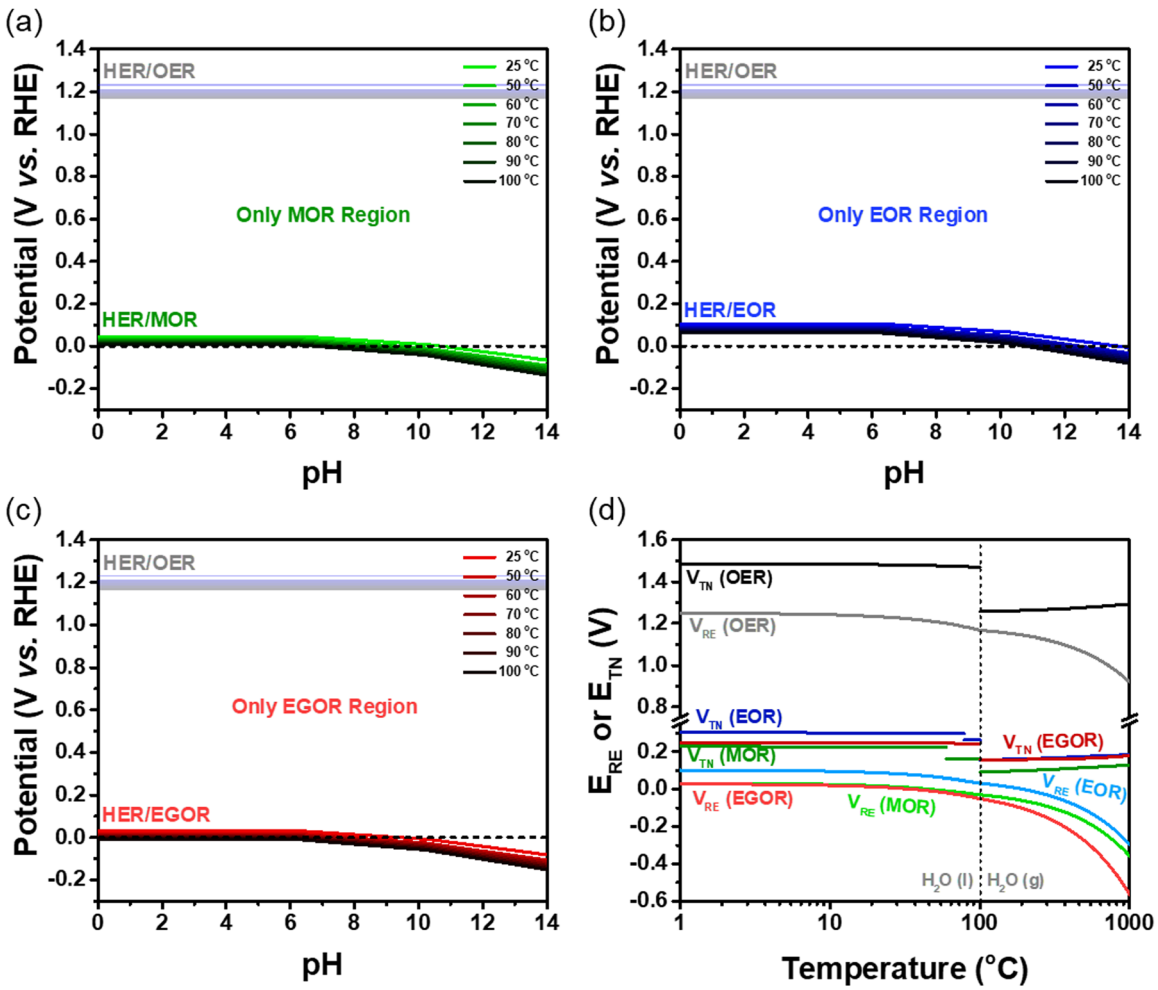

Fig. 8 Potential difference between water electrolysis and assisted water electrolysis using (a) methanol, (b) ethanol, and (c) ethylene glycol as a function of temperature from 25 to 100 °C. (d) V_{RE} and V_{TN} of water electrolysis and assisted water electrolysis using alcohols as a function of temperature from (0 to 1000 °C).

Similarly, the ethanol oxidation reaction follows trends comparable to HER but requires an additional potential input (Fig. 8(b)). At 25 °C, the required potentials for HER/EOR are 0.105 V at pH 0 and −0.007 V at pH 14. As the temperature increases to 100 °C, these values decrease to 0.063 V at pH 0 and −0.080 V at pH 14. The oxidation of ethylene glycol follows a similar trend, requiring the lowest energy input among alcohol oxidation reactions (Fig. 8(c)). The oxidation potentials shift with pH, and the potential gap relative to water electrolysis increases significantly in strongly alkaline environments. At 25 °C, the required potentials for HER/EGOR are 0.030 V at pH 0 and −0.081 V at pH 14. As the temperature increases to 100 °C, these values decrease to −0.009 V at pH 0 and −0.151 V at pH 14. This significant potential difference between water electrolysis and AWE using alcohols highlights the potential for energy-saving strategies in electrochemical hydrogen production. While V_{RE} and V_{TN} are widely used to evaluate water electrolysis efficiency, their application in the AWE field remains limited.

In particular, temperature-dependent theoretical potentials for AWE have not been thoroughly investigated. Fig. 8(d) compares the V_{TN} and V_{RE} values of MOR, EOR, and EGOR with those of OER across a broad temperature range (0–1000 °C). The results indicate that the V_{TN} values at 25 °C for MOR (0.226 V), EOR (0.301 V), and EGOR (0.248 V) are significantly lower than that of OER (1.481 V), highlighting the energetic advantage of organic oxidation in reducing the required electrolysis voltage. Similarly, the V_{RE} values at 25 °C for MOR (0.016 V), EOR (0.084 V), and EGOR (0.009 V) are also considerably lower than that of OER (1.229 V). As temperature increases, V_{RE} decreases, reducing the energy demand for assisted electrolysis, whereas V_{TN} increases, indicating that enthalpic benefits remain unchanged at elevated temperatures. Given that the oxidation potential of organic compounds is substantially lower than that of OER, organic oxidation can be selectively promoted while simultaneously suppressing OER as a competing side reaction.

The simulated results confirm that AWE using organic compounds effectively reduces the energy input required for hydrogen production. Replacing OER with organic oxidation can significantly reduce the total cell voltage, thereby improving overall energy efficiency and lowering operational costs for large-scale electrolysis applications. Furthermore, since many industrial processes generate waste alcohols and other organic compounds, AWE offers a sustainable approach to utilizing these byproducts for hydrogen production. This thermodynamic framework, which integrates Pourbaix diagrams and theoretical voltage calculations, provides a systematic approach for selecting optimal organic compounds and operating conditions for AWE.

Conclusion

This study presents a comprehensive thermodynamic framework for understanding electrochemical CO_2 conversion, encompassing CO_2RR and AWE under varying temperature (0–1000 °C) and pH conditions. By integrating Pourbaix diagrams and theoretical potentials (V_{TN} and V_{RE}), this work systematically evaluates the thermodynamic feasibility, equilibrium potential shifts, and reaction selectivity across different electrochemical environments. The results highlight the critical role of CO_2 phase transitions in governing reaction selectivity and energy efficiency.

Based on the comprehensive thermodynamic analysis presented in this work, we summarize the optimal conditions for the selective conversion of CO_2 to various products. Hydrocarbon formation (*e.g.*, CH_4, C_2H_4) is thermodynamically favorable under low to moderate pH and temperature (<100 °C), exhibiting higher theoretical potentials than HER under these conditions. Organic acids, such as HCOOH and CH_3COOH, exhibit specific thermodynamic selectivity windows, particularly in the pH range of 6–10, and are less susceptible to HER competition at low to intermediate temperatures. Alcohols (*e.g.*, CH_3OH, C_2H_5OH) exhibit higher sensitivity to temperature variations, with selective formation favored under mildly acidic and low-temperature conditions.

Furthermore, in addition to their thermodynamic advantages, acidic to neutral pH conditions also offer practical benefits for system operation. Under strongly alkaline conditions, the formation of alkali metal (bi)carbonate salts can cause precipitation, potentially clogging the flow channels of the electrolyzer and hindering long-term operational stability.[6] These results provide guidance for identifying suitable operating conditions for CO_2RR, enabling the rational design of reaction environments tailored for product-specific selectivity within a thermodynamic framework.

This thermodynamic understanding is not limited to CO_2RR. Beyond CO_2RR, this study highlights that phase-dependent shifts in equilibrium potential also play a critical role in AWE, where organic oxidation replaces the conventional OER. The V_{TN} and V_{RE} of organic oxidation reactions remain significantly lower than those of OER across a wide temperature range, reaffirming the energetic advantage of AWE. Furthermore, under strongly alkaline conditions, AWE becomes even more thermodynamically favorable due to the enhanced deprotonation of organic species and the shift of carbonate equilibria ($CO_2 \rightleftharpoons HCO_3^- \rightleftharpoons CO_3^{2-}$). This behavior contrasts with CO_2RR, where increasing alkalinity leads to a decrease in thermodynamic favorability, reflecting the fundamentally opposite nature of oxidation and reduction reactions.

This study integrates temperature-dependent Pourbaix diagrams with equilibrium potential modeling to further strengthen the thermodynamic predictions and provide a unified perspective. These insights highlight the crucial role of thermodynamics in guiding pathway selection, mitigating overpotentials, and improving overall energy efficiency in electrochemical systems. These findings are particularly relevant for enhancing CO_2RR selectivity, improving organic-assisted water electrolysis, and reducing energy demands in electrochemical hydrogen production.

Author contributions

J. C.: conceptualization, data curation, investigation, methodology, software, visualization, writing—original draft preparation, writing – review, and editing. H. L.: conceptualization, investigation, writing – original draft preparation, writing – review, and editing. S. S.: supervision, validation, visualization, writing – review, and editing. S. P.: resources, visualization, writing – review, and editing. J. S: resources, visualization, writing – review, and editing. G. H. J.: visualization, supervision, validation, writing – review, and editing. U. S.: conceptualization, investigation, visualization, supervision, funding acquisition, validation, writing – original draft preparation, writing – review, and editing.

Data availability

The data that support the findings of this study are included in the published article and its ESI.† The raw data are also available from the corresponding authors upon request.

Conflicts of interest

There are no conflicts to declare.

Acknowledgements

This work was supported by the National Research Foundation of Korea grant funded by the Ministry of Science and the Korean Government (MSIT), Republic of Korea (NRF-2021M3H4A6A01045764) and Korea Institute of Energy Technology Evaluation and Planning (KETEP) granted financial resources from Ministry of Trade, Industry & Energy, Republic of Korea (No. 20224000000320). This work was also supported by the Henan Center for Outstanding Overseas Scientists (GZS2024020).

References

1 Y. Y. Birdja, E. Pérez-Gallent, M. C. Figueiredo, A. J. Göttle, F. Calle-Vallejo and M. T. M. Koper, Advances and challenges in understanding the electrocatalytic conversion of carbon dioxide to fuels, *Nat. Energy*, 2019, **4**, 732–745.

2 C. Xu, P. Hong, Y. Dong, M. Robert, G. Shao and Y. Lei, Toward Complete CO_2 Electroconversion: Status, Challenges, and Perspectives, *Adv. Energy Mater.*, 2025, 2406146.

3 J. Li, Y. Ma, X. Mu, X. Wang, Y. Li, H. Ma and Z. Guo, Recent Advances and Perspectives on Coupled Water Electrolysis for Energy-Saving Hydrogen Production, *Adv. Sci.*, 2025, **12**, 2411964.

4 H. Choi, D.-K. Lee, M.-K. Han, G. Janani, S. Surendran, J. H. Kim, J. K. Kim, H. Cho and U. Sim, Review—Non-Noble Metal-Based Single-Atom Catalysts for Efficient Electrochemical CO_2 Reduction Reaction, *J. Electrochem. Soc.*, 2020, **167**, 164503.

5 H.-Y. Jeong, M. Balamurugan, V. S. K. Choutipalli, E.-S. Jeong, V. Subramanian, U. Sim and K. T. Nam, Achieving highly efficient CO_2 to CO electroreduction exceeding 300 mA cm^{-2} with single-atom nickel electrocatalysts, *J. Mater. Chem. A*, 2019, **7**, 10651–10661.

6 T. H. Ha, J. Kim, H. Choi and J. Oh, Selective Zero-Gap CO2 Reduction in Acid, *ACS Energy Lett.*, 2024, **9**, 4835–4842.

7 Z. Zhu, W. Tang, J. Wang, L. Zhao, Y. Lin, Z. Li, X. Niu, J. S. Chen and R. Wu, Insights into Operating Conditions on Electrocatalytic CO_2 Reduction, *Adv. Energy Mater.*, 2025, 2405768.

8 Y. Wang, D. Zhang, B. Sun, X. Jia, L. Zhang, H. Cheng, J. Fan and H. Li, Divergent Activity Shifts of Tin-Based Catalysts for Electrochemical CO_2 Reduction: pH-Dependent Behavior of Single-Atom *Versus* Polyatomic Structures, *Angew. Chem., Int. Ed.*, 2025, **64**, e202418228.

9 C. Jo, S. Surendran, M.-C. Kim, T.-Y. An, Y. Lim, H. Choi, G. Janani, S. Cyril Jesudass, D. Jun Moon, J. Kim, J. Young Kim, C. Hyuck Choi, M. Kim, J. Kyu Kim and U. Sim, Meticulous integration of N and C active sites in Ni_2P electrocatalyst for sustainable ammonia oxidation and efficient hydrogen production, *Chem. Eng. J.*, 2023, **463**, 142314.

10 H. Choi, S. Surendran, D. Kim, Y. Lim, J. Lim, J. Park, J. K. Kim, M.-K. Han and U. Sim, Boosting eco-friendly hydrogen generation by urea-assisted water electrolysis using spinel M_2GeO_4 (M = Fe, Co) as an active electrocatalyst, *Environ. Sci.: Nano*, 2021, **8**, 3110–3121.

11 H. Choi, M. G. Ha, J. Suh, C. Lim, B. Kim, S. E. Wang, J. Y. Lee, H.-S. Oh and J. Oh, Effect of the nitrogen/carbon ratio in the organic ligand of a nickel single-atom catalyst on its electrochemical activity in CO_2 reduction, *Appl. Catal., B*, 2024, **355**, 124192.

12 Y. Li, H. Zhang, T. Chen, Y. Sun, F. Rosei and M. Yu, Dual-Interfacial Electrocatalyst Enriching Surface Bonded H for Energy-Efficient CO_2-to-CH_3OH Conversion, *Adv. Funct. Mater.*, 2024, **34**, 2312970.

13 J. Choi, H. Lim, S. Surendran, X. Lu, K. Jin, H. Park, H.-Y. Jung and U. Sim, Dichalcogenides as Emerging Electrocatalysts for Efficient Ammonia Synthesis: A Focus on Mechanisms and Theoretical Potentials, *Adv. Funct. Mater.*, 2025, 2422585.

14 M. König, J. Vaes, E. Klemm and D. Pant, Solvents and Supporting Electrolytes in the Electrocatalytic Reduction of CO_2, *iScience*, 2019, **19**, 135–160.

15 P. W. Atkins, J. De Paula and J. Keeler, *Atkins' physical chemistry*, Oxford University Press, 2023.

16 J. Choi, S. Yoo, G. Janani, S. Surendran, S. Shanmugapriya, H. Choi, G. Kwon, K. Jin and U. Sim, Recent research trends in the rational designing of single atom catalysts for electrochemical CO_2 reduction reaction to CO—a mini review, *Carbon Lett.*, 2025, **35**, 469–479.

17 H. Song, C. A. Fernández, H. Choi, P.-W. Huang, J. Oh and M. C. Hatzell, Integrated carbon capture and CO production from bicarbonates through bipolar membrane electrolysis, *Energy Environ. Sci.*, 2024, **17**, 3570–3579.

18 B. Kim, Y. C. Tan, Y. Ryu, K. Jang, H. G. Abbas, T. Kang, H. Choi, K.-S. Lee, S. Park, W. Kim, P.-P. Choi, S. Ringe and J. Oh, Trace-Level Cobalt Dopants Enhance CO_2 Electroreduction and Ethylene Formation on Copper, *ACS Energy Lett.*, 2023, **8**, 3356–3364.

19 Y. Kim, B. Kim, H. Choi, S. Kim, Y. Yun and J. Oh, Modulating the electronic structure of Au using a heterostructure for efficient electrochemical CO_2 reduction, *Chem. Eng. J.*, 2023, **461**, 142126.
20 W. Ma, X. He, W. Wang, S. Xie, Q. Zhang and Y. Wang, Electrocatalytic reduction of CO_2 and CO to multi-carbon compounds over Cu-based catalysts, *Chem. Soc. Rev.*, 2021, **50**, 12897–12914.
21 X. Zhang, W. Huang, L. Yu, M. García-Melchor, D. Wang, L. Zhi and H. Zhang, Enabling heterogeneous catalysis to achieve carbon neutrality: Directional catalytic conversion of CO2 into carboxylic acids, *Carbon Energy*, 2024, **6**, e362.
22 H. Shen, H. Jin, H. Li, H. Wang, J. Duan, Y. Jiao and S.-Z. Qiao, Acidic CO_2-to-HCOOH electrolysis with industrial-level current on phase engineered tin sulfide, *Nat. Commun.*, 2023, **14**, 2843.
23 Q. Zhu, X. Sun, D. Yang, J. Ma, X. Kang, L. Zheng, J. Zhang, Z. Wu and B. Han, Carbon dioxide electroreduction to C_2 products over copper–cuprous oxide derived from electrosynthesized copper complex, *Nat. Commun.*, 2019, **10**, 3851.
24 S. Wang, H. D. Jung, H. Choi, J. Kim, S. Back and J. Oh, Delicate control of a gold-copper oxide tandem structure enables the efficient production of high-value chemicals by electrochemical carbon dioxide reduction, *Nano Energy*, 2024, **130**, 110176.
25 C. Guo, Y. Guo, Y. Shi, X. Lan, Y. Wang, Y. Yu and B. Zhang, Electrocatalytic Reduction of CO_2 to Ethanol at Close to Theoretical Potential via Engineering Abundant Electron-Donating Cu^+ Species, *Angew. Chem., Int. Ed.*, 2022, **61**, e202205909.
26 F. Arshad, Tu Haq, I. Hussain and F. Sher, Recent Advances in Electrocatalysts toward Alcohol-Assisted, Energy-Saving Hydrogen Production, *ACS Appl. Energy Mater.*, 2021, **4**, 8685–8701.
27 F. Liu, T. Wang, J. Li, T. Wei, Z. Ye, D. Dong, B. Chen, Y. Ling and Z. Shao, Elevated-temperature bio-ethanol-assisted water electrolysis for efficient hydrogen production, *Chem. Eng. J.*, 2022, **434**, 134699.
28 Q. Liu, S. Du, T. Liu, L. Gong, Y. Wu, J. Lin, P. Yang, G. Huang, M. Li, Y. Wu, Y. Zhou, Y. Li, L. Tao and S. Wang, Efficient Low-temperature Hydrogen Production by Electrochemical-assisted Methanol Steam Reforming, *Angew. Chem., Int. Ed.*, 2024, **63**, e202315157.
29 Q. Mao, K. Deng, H. Yu, Y. Xu, Z. Wang, X. Li, L. Wang and H. Wang, *In Situ* Reconstruction of Partially Hydroxylated Porous Rh Metallene for Ethylene Glycol-Assisted Seawater Splitting, *Adv. Funct. Mater.*, 2022, **32**, 2201081.

